

This is the accepted manuscript made available via CHORUS. The article has been published as:

## Searches for Sterile Neutrinos with the IceCube Detector

M. G. Aartsen *et al.* (IceCube Collaboration)

Phys. Rev. Lett. **117**, 071801 — Published 8 August 2016

DOI: [10.1103/PhysRevLett.117.071801](https://doi.org/10.1103/PhysRevLett.117.071801)

# 1 Searches for Sterile Neutrinos with the IceCube Detector

2 M. G. Aartsen,<sup>2</sup> K. Abraham,<sup>35</sup> M. Ackermann,<sup>53</sup> J. Adams,<sup>16</sup> J. A. Aguilar,<sup>12</sup> M. Ahlers,<sup>30</sup> M. Ahrens,<sup>43</sup>  
3 D. Altmann,<sup>24</sup> K. Andeen,<sup>32</sup> T. Anderson,<sup>49</sup> I. Ansseau,<sup>12</sup> G. Anton,<sup>24</sup> M. Archinger,<sup>31</sup> C. Argüelles,<sup>14</sup>  
4 T. C. Arlen,<sup>49</sup> J. Auffenberg,<sup>1</sup> S. Axani,<sup>14</sup> X. Bai,<sup>41</sup> S. W. Barwick,<sup>27</sup> V. Baum,<sup>31</sup> R. Bay,<sup>7</sup> J. J. Beatty,<sup>18, 19</sup>  
5 J. Becker Tjus,<sup>10</sup> K.-H. Becker,<sup>52</sup> S. BenZvi,<sup>50</sup> P. Berghaus,<sup>34</sup> D. Berley,<sup>17</sup> E. Bernardini,<sup>53</sup> A. Bernhard,<sup>35</sup>  
6 D. Z. Besson,<sup>28</sup> G. Binder,<sup>8, 7</sup> D. Bindig,<sup>52</sup> E. Blaufuss,<sup>17</sup> S. Blot,<sup>53</sup> D. J. Boersma,<sup>51</sup> C. Bohm,<sup>43</sup> M. Börner,<sup>21</sup>  
7 F. Bos,<sup>10</sup> D. Bose,<sup>45</sup> S. Böser,<sup>31</sup> O. Botner,<sup>51</sup> J. Braun,<sup>30</sup> L. Brayer,<sup>13</sup> H.-P. Bretz,<sup>53</sup> A. Burgman,<sup>51</sup>  
8 J. Casey,<sup>5</sup> M. Casier,<sup>13</sup> E. Cheung,<sup>17</sup> D. Chirkin,<sup>30</sup> A. Christov,<sup>25</sup> K. Clark,<sup>46</sup> L. Classen,<sup>36</sup> S. Coenders,<sup>35</sup>  
9 G. H. Collin,<sup>14</sup> J. M. Conrad,<sup>14</sup> D. F. Cowen,<sup>49, 48</sup> A. H. Cruz Silva,<sup>53</sup> J. Daughhetee,<sup>5</sup> J. C. Davis,<sup>18</sup> M. Day,<sup>30</sup>  
10 J. P. A. M. de André,<sup>22</sup> C. De Clercq,<sup>13</sup> E. del Pino Rosendo,<sup>31</sup> H. Dembinski,<sup>37</sup> S. De Ridder,<sup>26</sup> P. Desiati,<sup>30</sup>  
11 K. D. de Vries,<sup>13</sup> G. de Wasseige,<sup>13</sup> M. de With,<sup>9</sup> T. DeYoung,<sup>22</sup> J. C. Díaz-Vélez,<sup>30</sup> V. di Lorenzo,<sup>31</sup>  
12 H. Dujmovic,<sup>45</sup> J. P. Dumm,<sup>43</sup> M. Dunkman,<sup>49</sup> B. Eberhardt,<sup>31</sup> T. Ehrhardt,<sup>31</sup> B. Eichmann,<sup>10</sup> S. Euler,<sup>51</sup>  
13 P. A. Evenson,<sup>37</sup> S. Fahey,<sup>30</sup> A. R. Fazely,<sup>6</sup> J. Feintzeig,<sup>30</sup> J. Felde,<sup>17</sup> K. Filimonov,<sup>7</sup> C. Finley,<sup>43</sup> S. Flis,<sup>43</sup>  
14 C.-C. Fösig,<sup>31</sup> T. Fuchs,<sup>21</sup> T. K. Gaisser,<sup>37</sup> R. Gaior,<sup>15</sup> J. Gallagher,<sup>29</sup> L. Gerhardt,<sup>8, 7</sup> K. Ghorbani,<sup>30</sup> W. Giang,<sup>23</sup>  
15 L. Gladstone,<sup>30</sup> T. Glüsenkamp,<sup>53</sup> A. Goldschmidt,<sup>8</sup> G. Golup,<sup>13</sup> J. G. Gonzalez,<sup>37</sup> D. Góra,<sup>53</sup> D. Grant,<sup>23</sup>  
16 Z. Griffith,<sup>30</sup> A. Haj Ismail,<sup>26</sup> A. Hallgren,<sup>51</sup> F. Halzen,<sup>30</sup> E. Hansen,<sup>20</sup> K. Hanson,<sup>30</sup> D. Heebecker,<sup>9</sup> D. Heereman,<sup>12</sup>  
17 K. Helbing,<sup>52</sup> R. Hellauer,<sup>17</sup> S. Hickford,<sup>52</sup> J. Hignight,<sup>22</sup> G. C. Hill,<sup>2</sup> K. D. Hoffman,<sup>17</sup> R. Hoffmann,<sup>52</sup>  
18 K. Holzapfel,<sup>35</sup> A. Homeier,<sup>11</sup> K. Hoshina,<sup>30, \*</sup> F. Huang,<sup>49</sup> M. Huber,<sup>35</sup> W. Huelsnitz,<sup>17</sup> K. Hultqvist,<sup>43</sup>  
19 S. In,<sup>45</sup> A. Ishihara,<sup>15</sup> E. Jacobi,<sup>53</sup> G. S. Japaridze,<sup>4</sup> M. Jeong,<sup>45</sup> K. Jero,<sup>30</sup> B. J. P. Jones,<sup>14</sup> M. Jurkovic,<sup>35</sup>  
20 A. Kappes,<sup>36</sup> T. Karg,<sup>53</sup> A. Karle,<sup>30</sup> U. Katz,<sup>24</sup> M. Kauer,<sup>30, 38</sup> A. Keivani,<sup>49</sup> J. L. Kelley,<sup>30</sup> A. Kheirandish,<sup>30</sup>  
21 M. Kim,<sup>45</sup> T. Kintscher,<sup>53</sup> J. Kiryluk,<sup>44</sup> T. Kittler,<sup>24</sup> S. R. Klein,<sup>8, 7</sup> G. Kohnen,<sup>33</sup> R. Koirala,<sup>37</sup> H. Kolanoski,<sup>9</sup>  
22 L. Köpke,<sup>31</sup> C. Kopper,<sup>23</sup> S. Kopper,<sup>52</sup> D. J. Koskinen,<sup>20</sup> M. Kowalski,<sup>9, 53</sup> K. Krings,<sup>35</sup> M. Kroll,<sup>10</sup> G. Krückl,<sup>31</sup>  
23 C. Krüger,<sup>30</sup> J. Kunnen,<sup>13</sup> S. Kunwar,<sup>53</sup> N. Kurahashi,<sup>40</sup> T. Kuwabara,<sup>15</sup> M. Labare,<sup>26</sup> J. L. Lanfranchi,<sup>49</sup>  
24 M. J. Larson,<sup>20</sup> D. Lennarz,<sup>22</sup> M. Lesiak-Bzdak,<sup>44</sup> M. Leuermann,<sup>1</sup> L. Lu,<sup>15</sup> J. Lünemann,<sup>13</sup> J. Madsen,<sup>42</sup>  
25 G. Maggi,<sup>13</sup> K. B. M. Mahn,<sup>22</sup> S. Mancina,<sup>30</sup> M. Mandelartz,<sup>10</sup> R. Maruyama,<sup>38</sup> K. Mase,<sup>15</sup> R. Maunu,<sup>17</sup>  
26 F. McNally,<sup>30</sup> K. Meagher,<sup>12</sup> M. Medici,<sup>20</sup> M. Meier,<sup>21</sup> A. Meli,<sup>26</sup> T. Menne,<sup>21</sup> G. Merino,<sup>30</sup> T. Meures,<sup>12</sup>  
27 S. Miarecki,<sup>8, 7</sup> E. Middell,<sup>53</sup> L. Mohrmann,<sup>53</sup> T. Montaruli,<sup>25</sup> M. Moulai,<sup>14</sup> R. Nahnauer,<sup>53</sup> U. Naumann,<sup>52</sup>  
28 G. Neer,<sup>22</sup> H. Niederhausen,<sup>44</sup> S. C. Nowicki,<sup>23</sup> D. R. Nygren,<sup>8</sup> A. Obertacke Pollmann,<sup>52</sup> A. Olivas,<sup>17</sup>  
29 A. Omairat,<sup>52</sup> A. O'Murchadha,<sup>12</sup> T. Palczewski,<sup>47</sup> H. Pandya,<sup>37</sup> D. V. Pankova,<sup>49</sup> J. A. Pepper,<sup>47</sup>  
30 C. Pérez de los Heros,<sup>51</sup> C. Pfendner,<sup>18</sup> D. Pieloth,<sup>21</sup> E. Pinat,<sup>12</sup> J. Posselt,<sup>52</sup> P. B. Price,<sup>7</sup> G. T. Przybylski,<sup>8</sup>  
31 M. Quinnan,<sup>49</sup> C. Raab,<sup>12</sup> M. Rameez,<sup>25</sup> K. Rawlins,<sup>3</sup> M. Relich,<sup>15</sup> E. Resconi,<sup>35</sup> W. Rhode,<sup>21</sup> M. Richman,<sup>40</sup>  
32 B. Riedel,<sup>23</sup> S. Robertson,<sup>2</sup> C. Rott,<sup>45</sup> T. Ruhe,<sup>21</sup> D. Ryckbosch,<sup>26</sup> D. Rysewyk,<sup>22</sup> L. Sabbatini,<sup>30</sup> J. Salvado,<sup>30, †</sup>  
33 S. E. Sanchez Herrera,<sup>23</sup> A. Sandrock,<sup>21</sup> J. Sandroos,<sup>31</sup> S. Sarkar,<sup>20, 39</sup> K. Satalecka,<sup>53</sup> P. Schlunder,<sup>21</sup> T. Schmidt,<sup>17</sup>  
34 S. Schöneberg,<sup>10</sup> A. Schönwald,<sup>53</sup> D. Seckel,<sup>37</sup> S. Seunarine,<sup>42</sup> D. Soldin,<sup>52</sup> M. Song,<sup>17</sup> G. M. Spiczak,<sup>42</sup>  
35 C. Spiering,<sup>53</sup> M. Stamatikos,<sup>18, †</sup> T. Staney,<sup>37</sup> A. Stasik,<sup>53</sup> A. Steuer,<sup>31</sup> T. Stezelberger,<sup>8</sup> R. G. Stokstad,<sup>8</sup>  
36 A. Stößl,<sup>53</sup> R. Ström,<sup>51</sup> N. L. Strotjohann,<sup>53</sup> G. W. Sullivan,<sup>17</sup> M. Sutherland,<sup>18</sup> H. Taavola,<sup>51</sup> I. Taboada,<sup>5</sup>  
37 J. Tatar,<sup>8, 7</sup> S. Ter-Antonyan,<sup>6</sup> A. Terliuk,<sup>53</sup> G. Tešić,<sup>49</sup> S. Tilav,<sup>37</sup> P. A. Toale,<sup>47</sup> M. N. Tobin,<sup>30</sup> S. Toscano,<sup>13</sup>  
38 D. Tosi,<sup>30</sup> M. Tselengidou,<sup>24</sup> A. Turcati,<sup>35</sup> E. Unger,<sup>51</sup> M. Usner,<sup>53</sup> S. Vallecorsa,<sup>25</sup> J. Vandebroucke,<sup>30</sup>  
39 N. van Eijndhoven,<sup>13</sup> S. Vanheule,<sup>26</sup> M. van Rossem,<sup>30</sup> J. van Santen,<sup>53</sup> J. Veenkamp,<sup>35</sup> M. Voge,<sup>11</sup> M. Vraeghe,<sup>26</sup>  
40 C. Walck,<sup>43</sup> A. Wallace,<sup>2</sup> N. Wandkowsky,<sup>30</sup> Ch. Weaver,<sup>23</sup> C. Wendt,<sup>30</sup> S. Westerhoff,<sup>30</sup> B. J. Whelan,<sup>2</sup>  
41 K. Wiebe,<sup>31</sup> L. Wille,<sup>30</sup> D. R. Williams,<sup>47</sup> L. Wills,<sup>40</sup> H. Wissing,<sup>17</sup> M. Wolf,<sup>43</sup> T. R. Wood,<sup>23</sup> E. Woolsey,<sup>23</sup>  
42 K. Woschnagg,<sup>7</sup> D. L. Xu,<sup>30</sup> X. W. Xu,<sup>6</sup> Y. Xu,<sup>44</sup> J. P. Yanez,<sup>53</sup> G. Yodh,<sup>27</sup> S. Yoshida,<sup>15</sup> and M. Zoll<sup>43</sup>

43 (IceCube Collaboration)<sup>§</sup>

44 <sup>1</sup>III. Physikalisches Institut, RWTH Aachen University, D-52056 Aachen, Germany

45 <sup>2</sup>Department of Physics, University of Adelaide, Adelaide, 5005, Australia

46 <sup>3</sup>Dept. of Physics and Astronomy, University of Alaska Anchorage, 3211 Providence Dr., Anchorage, AK 99508, USA

47 <sup>4</sup>CTSPS, Clark-Atlanta University, Atlanta, GA 30314, USA

48 <sup>5</sup>School of Physics and Center for Relativistic Astrophysics, Georgia Institute of Technology, Atlanta, GA 30332, USA

49 <sup>6</sup>Dept. of Physics, Southern University, Baton Rouge, LA 70813, USA

50 <sup>7</sup>Dept. of Physics, University of California, Berkeley, CA 94720, USA

51 <sup>8</sup>Lawrence Berkeley National Laboratory, Berkeley, CA 94720, USA

52 <sup>9</sup>Institut für Physik, Humboldt-Universität zu Berlin, D-12489 Berlin, Germany

- <sup>10</sup>*Fakultät für Physik & Astronomie, Ruhr-Universität Bochum, D-44780 Bochum, Germany*
- <sup>11</sup>*Physikalisches Institut, Universität Bonn, Nussallee 12, D-53115 Bonn, Germany*
- <sup>12</sup>*Université Libre de Bruxelles, Science Faculty CP230, B-1050 Brussels, Belgium*
- <sup>13</sup>*Vrije Universiteit Brussel, Dienst ELEM, B-1050 Brussels, Belgium*
- <sup>14</sup>*Dept. of Physics, Massachusetts Institute of Technology, Cambridge, MA 02139, USA*
- <sup>15</sup>*Dept. of Physics, Chiba University, Chiba 263-8522, Japan*
- <sup>16</sup>*Dept. of Physics and Astronomy, University of Canterbury, Private Bag 4800, Christchurch, New Zealand*
- <sup>17</sup>*Dept. of Physics, University of Maryland, College Park, MD 20742, USA*
- <sup>18</sup>*Dept. of Physics and Center for Cosmology and Astro-Particle Physics, Ohio State University, Columbus, OH 43210, USA*
- <sup>19</sup>*Dept. of Astronomy, Ohio State University, Columbus, OH 43210, USA*
- <sup>20</sup>*Niels Bohr Institute, University of Copenhagen, DK-2100 Copenhagen, Denmark*
- <sup>21</sup>*Dept. of Physics, TU Dortmund University, D-44221 Dortmund, Germany*
- <sup>22</sup>*Dept. of Physics and Astronomy, Michigan State University, East Lansing, MI 48824, USA*
- <sup>23</sup>*Dept. of Physics, University of Alberta, Edmonton, Alberta, Canada T6G 2E1*
- <sup>24</sup>*Erlangen Centre for Astroparticle Physics, Friedrich-Alexander-Universität Erlangen-Nürnberg, D-91058 Erlangen, Germany*
- <sup>25</sup>*Département de physique nucléaire et corpusculaire, Université de Genève, CH-1211 Genève, Switzerland*
- <sup>26</sup>*Dept. of Physics and Astronomy, University of Gent, B-9000 Gent, Belgium*
- <sup>27</sup>*Dept. of Physics and Astronomy, University of California, Irvine, CA 92697, USA*
- <sup>28</sup>*Dept. of Physics and Astronomy, University of Kansas, Lawrence, KS 66045, USA*
- <sup>29</sup>*Dept. of Astronomy, University of Wisconsin, Madison, WI 53706, USA*
- <sup>30</sup>*Dept. of Physics and Wisconsin IceCube Particle Astrophysics Center, University of Wisconsin, Madison, WI 53706, USA*
- <sup>31</sup>*Institute of Physics, University of Mainz, Staudinger Weg 7, D-55099 Mainz, Germany*
- <sup>32</sup>*Department of Physics, Marquette University, Milwaukee, WI, 53201, USA*
- <sup>33</sup>*Université de Mons, 7000 Mons, Belgium*
- <sup>34</sup>*National Research Nuclear University MEPhI (Moscow Engineering Physics Institute), Moscow, Russia*
- <sup>35</sup>*Physik-department, Technische Universität München, D-85748 Garching, Germany*
- <sup>36</sup>*Institut für Kernphysik, Westfälische Wilhelms-Universität Münster, D-48149 Münster, Germany*
- <sup>37</sup>*Bartol Research Institute and Dept. of Physics and Astronomy, University of Delaware, Newark, DE 19716, USA*
- <sup>38</sup>*Dept. of Physics, Yale University, New Haven, CT 06520, USA*
- <sup>39</sup>*Dept. of Physics, University of Oxford, 1 Keble Road, Oxford OX1 3NP, UK*
- <sup>40</sup>*Dept. of Physics, Drexel University, 3141 Chestnut Street, Philadelphia, PA 19104, USA*
- <sup>41</sup>*Physics Department, South Dakota School of Mines and Technology, Rapid City, SD 57701, USA*
- <sup>42</sup>*Dept. of Physics, University of Wisconsin, River Falls, WI 54022, USA*
- <sup>43</sup>*Oskar Klein Centre and Dept. of Physics, Stockholm University, SE-10691 Stockholm, Sweden*
- <sup>44</sup>*Dept. of Physics and Astronomy, Stony Brook University, Stony Brook, NY 11794-3800, USA*
- <sup>45</sup>*Dept. of Physics, Sungkyunkwan University, Suwon 440-746, Korea*
- <sup>46</sup>*Dept. of Physics, University of Toronto, Toronto, Ontario, Canada, M5S 1A7*
- <sup>47</sup>*Dept. of Physics and Astronomy, University of Alabama, Tuscaloosa, AL 35487, USA*
- <sup>48</sup>*Dept. of Astronomy and Astrophysics, Pennsylvania State University, University Park, PA 16802, USA*
- <sup>49</sup>*Dept. of Physics, Pennsylvania State University, University Park, PA 16802, USA*
- <sup>50</sup>*Dept. of Physics and Astronomy, University of Rochester, Rochester, NY 14627, USA*
- <sup>51</sup>*Dept. of Physics and Astronomy, Uppsala University, Box 516, S-75120 Uppsala, Sweden*
- <sup>52</sup>*Dept. of Physics, University of Wuppertal, D-42119 Wuppertal, Germany*
- <sup>53</sup>*DESY, D-15735 Zeuthen, Germany*

(Dated: June 22, 2016)

The IceCube neutrino telescope at the South Pole has measured the atmospheric muon neutrino spectrum as a function of zenith angle and energy in the approximate 320 GeV to 20 TeV range, to search for the oscillation signatures of light sterile neutrinos. No evidence for anomalous  $\nu_\mu$  or  $\bar{\nu}_\mu$  disappearance is observed in either of two independently developed analyses, each using one year of atmospheric neutrino data. New exclusion limits are placed on the parameter space of the 3+1 model, in which muon antineutrinos would experience a strong MSW-resonant oscillation. The exclusion limits extend to  $\sin^2 2\theta_{24} \leq 0.02$  at  $\Delta m^2 \sim 0.3$  eV<sup>2</sup> at the 90% confidence level. The allowed region from global analysis of appearance experiments, including LSND and MiniBooNE, is excluded at approximately the 99% confidence level for the global best fit value of  $|U_{e4}|^2$ .

## INTRODUCTION

Sterile neutrinos with masses in the range  $\Delta m^2 = 0.1$  eV<sup>2</sup> – 10 eV<sup>2</sup> have been posited to explain anomalies in accelerator [1–3], reactor [4], and radioactive source [5] oscillation experiments. Several null results

[6–10] restrict the available parameter space of the minimal 3+1 model, which assumes mixing of the three active neutrinos with a single sterile neutrino, resulting in three light and one heavier mass state. Global fits to world data [11–13] demonstrate that there remain regions of allowed parameter space around the best fit point of

$\Delta m^2 = 1 \text{ eV}^2$  and  $\sin^2 2\theta_{24} = 0.1$ . A consequence of these models is the existence of  $\nu_\mu$  ( $\bar{\nu}_\mu$ ) disappearance signatures, which are yet to be observed.

Atmospheric neutrinos produced in cosmic ray air showers throughout the Earth's atmosphere are detected by IceCube [14]. To mitigate the large atmospheric muon background, only up-going neutrinos are selected. For these trajectories, the Earth acts as a filter to remove the charged particle background. At high neutrino energies, the Earth also modifies the neutrino flux due to charged current and neutral current interactions [15]. At  $E_\nu > 100 \text{ GeV}$ , oscillations due to the known neutrino mass splittings have wavelengths larger than the diameter of the Earth and can be neglected.

A previous measurement of the atmospheric flux in the sub-TeV range, performed by the Super-Kamiokande experiment, found no evidence for anomalous neutrino disappearance [7]. This paper reports the first searches for  $(\nu_\mu + \bar{\nu}_\mu)$  disappearance in the approximate 320 GeV to 20 TeV range, using two independent analyses each based on one-year data samples from the IceCube detector [16, 17]. In this energy regime, sterile neutrinos would produce distinctive energy-dependent distortions of the measured zenith angle distributions [18], caused by resonant matter-enhanced oscillations during neutrino propagation through the Earth.

This MSW resonant effect depletes antineutrinos in 3+1 models (or neutrinos in 1+3) [18, 19]. Additional oscillation effects produced by sterile neutrinos include vacuum-like oscillations at low energies for both neutrinos and antineutrinos, and a modification of the Earth opacity at high energies, as sterile neutrinos are unaffected by matter. These effects would lead to detectable distortions of the flux in energy and angle, henceforth called "shape effects," in IceCube for mass splittings in the range  $0.01 \text{ eV}^2 \leq \Delta m^2 \leq 10 \text{ eV}^2$  [20–27].

## ATMOSPHERIC NEUTRINOS IN ICECUBE

Having crossed the Earth, a small fraction of up-going atmospheric neutrinos undergo charged current interactions in either bedrock or ice, creating muons that traverse the instrumented ice of IceCube. These produce secondary particles that add Cherenkov light, which can be detected by the Digital Optical Modules (DOMs) [28–30] of the IceCube array. The full detector contains 5160 DOMs on 86 strings arranged with string-to-string spacing of approximately 125 m and typical vertical DOM separation of 17 m.

The analysis detailed in this paper, referred to as IC86, uses data from the full 86-string detector configuration taken during 2011–2012, with up-going neutrinos selected according to the procedure developed in [16, 31]. The sample contains 20,145 well-reconstructed muons detected over a live time of 343.7 days. A total of 99.9%

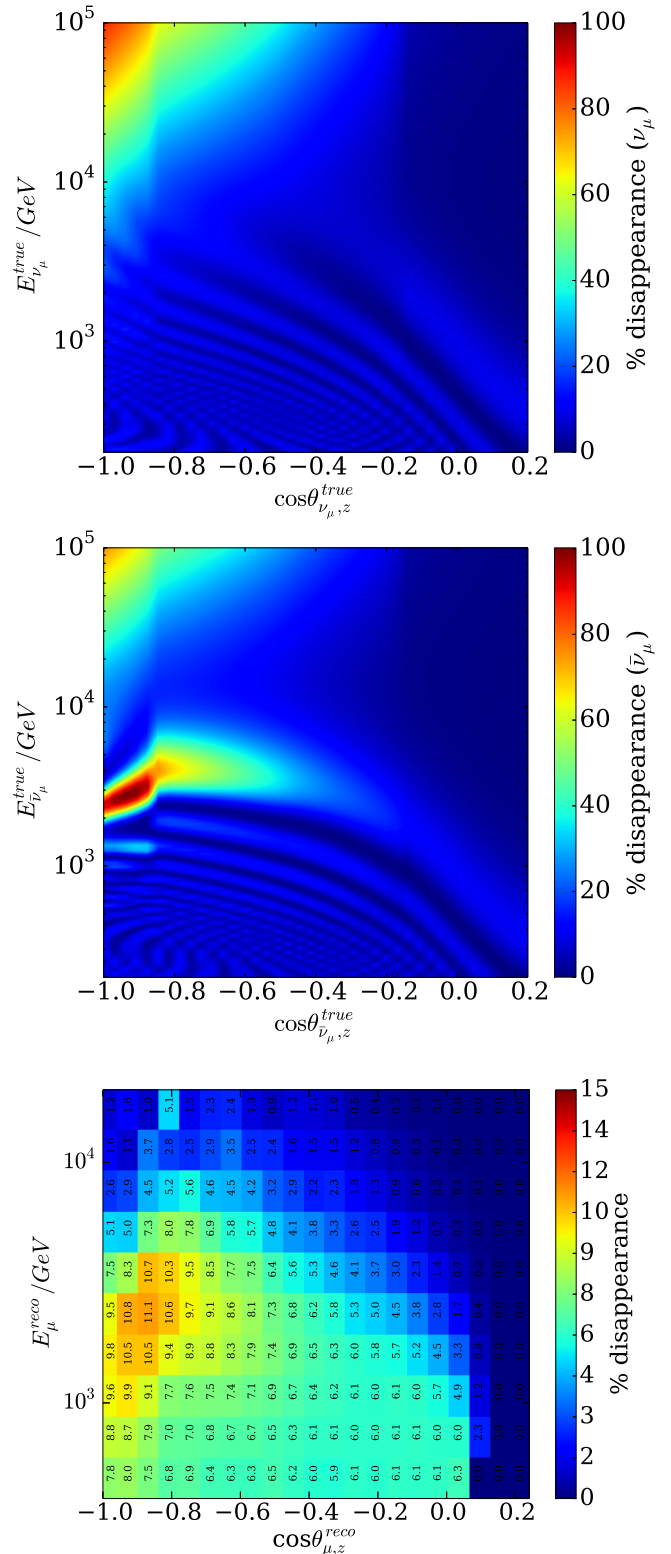


FIG. 1. Top and center: change in the spectrum due to propagation effects for muon neutrinos and antineutrinos at the 3+1 global best fit point. Bottom: The predicted event rate reduction (in percent) vs. reconstructed muon energy and zenith angle for this model.

of the detected events in the data sample are expected to be neutrino-induced muon events from the decays of atmospheric pions and kaons. The flux contribution from charmed meson decays was found to be negligible [16, 32], as was the contamination of up-going astrophysical neutrinos with the spectrum and rate measured by IceCube [16]. A complementary analysis, referred to as IC59 and discussed later, was performed using a sample of 21,857 events observed in 348.1 days of data taken with an earlier 59-string configuration of the detector from 2009–2010 [17].

Since muon production is very forward at these energies, the muon preserves the original neutrino direction with a median opening angle following  $0.7 \text{ degrees} \times (E_\nu/\text{TeV})^{-0.7}$  [33]. The muon zenith angle can be reconstructed geometrically with a resolution of  $\sigma_{\cos(\theta_z)}$  varying between 0.005 and 0.015 depending on the angle. Due to energy sharing in production and radiative losses outside the detector, the detected muon energy is smeared downward from the original neutrino value. Muon energy is reconstructed based on the stochastic light emission profile along the track [16, 34] with a resolution of  $\sigma_{\log_{10}(E_\mu/\text{GeV})} \sim 0.5$ .

To search for shape effects [22, 23, 25, 26], including the MSW and parametric resonances, the analyses compare the predicted observable muon spectrum for a given incident neutrino flux and oscillation hypothesis with data. Flavor evolution in the active and sterile neutrino system can be calculated by numerical solution of a master equation [15, 35]. For IC86, this calculation is performed using the  $\nu$ -SQuIDs software package [36, 37], while the IC59 analysis approximates the oscillation probability by solving a Schrödinger-like equation using the NuCraft package [38]. This approximation is accurate to better than 10% below  $\Delta m^2 \approx 5 \text{ eV}^2$ , where Earth-absorption effects can be neglected. Fig. 1 top and center show the  $\nu_\mu$  and  $\bar{\nu}_\mu$  oscillation probability vs. true energy and zenith angle, calculated at the best-fit point from [13]. Since IceCube has no sign-selection capability, the reconstructed samples contain both  $\mu^+$  and  $\mu^-$  events. For illustration, Fig. 1 (bottom) shows the predicted depletion of events for the global 3+1 best fit point in the distribution of reconstructed variables from the IC86 analysis; in this case the large depletion is dominated by the parametric resonance.

## DATA ANALYSIS AND SYSTEMATIC UNCERTAINTIES

To search for sterile neutrino oscillations we calculate the negative of a binned Poissonian log-likelihood (LLH) for the data given each sterile neutrino hypothesis on a fine grid in the the  $[\log(\Delta m^2), \log(\sin^2 2\theta_{24})]$  hypothesis space. In the IC86 analysis, the data are histogrammed on a grid with 10 bins in energy ranging from

400 GeV to 20 TeV, and 21 linearly spaced bins starting at  $\cos(\theta) = 0.24$  with a spacing of 0.06. The bins were chosen a priori guided by experimental resolution, scale of the disappearance signatures and accumulated MC simulation statistics. The LLH values are compared to the minimum in the space to produce unified confidence intervals [39]. Systematic uncertainties are treated by introducing both continuous and discrete nuisance parameters, which are fitted at each hypothesis point. The list of systematic uncertainties considered is given in Table I and discussed below. More information can be found in [40] and [41].

<i>Atmospheric flux</i>		
$\nu$ flux template	discrete	(7)
$\nu / \bar{\nu}$ ratio	continuous	0.025
$\pi / K$ ratio	continuous	0.1
Normalization	continuous	none <sup>1</sup>
Cosmic ray spectral index	continuous	0.05
Atmospheric temperature	continuous	model tuned
<i>Detector and ice model</i>		
DOM efficiency	continuous	
Ice properties	discrete	(4)
Hole ice effect on angular response	discrete	(2)
<i>Neutrino propagation and interaction</i>		
DIS cross section	discrete	(6)
Earth density	discrete	(9)

TABLE I. List of systematic uncertainties considered in the analysis. The numbers in parentheses show the number of discrete variants used. Full descriptions are given in the text. The third column indicates the gaussian width of a prior if introduced for the parameter in the analysis (see [40] for details). <sup>1</sup>A prior of 40% was applied to the Normalization parameter in the rate+shape analysis described below.

## Atmospheric neutrino flux uncertainties

The atmospheric flux in the energies relevant to this analysis is dominated by the neutrinos that originate from pion and kaon decays in cosmic ray showers. This prompts us to parametrize the atmospheric flux as

$$\phi_{\text{atm}}(\cos \theta) = N_0 \mathcal{F}(\delta) \left( \phi_\pi + R_{\pi/K} \phi_K \right) \left( \frac{E_\nu}{E_0} \right)^{-\Delta\gamma} \quad (1)$$

(and similarly for antineutrinos, with a relative flux normalization uncertainty). The free nuisance parameters are the overall flux normalization  $N_0$ , the correction to the ratio of kaon- to pion-induced fluxes  $R_{K/\pi}$  and the spectral index correction  $\Delta\gamma$ . The  $\phi_\pi$  and  $\phi_K$  are the spectrum of atmospheric neutrinos originating from  $\pi$  and  $K$  decays, respectively. Furthermore,  $\Delta\gamma$  allows us to take into account uncertainties in the spectral index of the flux. The term  $E_0$  is a pivot point near the median of

246 the energy distribution which renders the  $\Delta\gamma$  correction<sup>295</sup>  
 247 approximately normalization-conserving.

248 Here, seven  $\phi_k$  and  $\phi_\pi$  variants are used to encapsulate<sup>296</sup>  
 249 additional hadronic model uncertainty and the primary<sup>297</sup>  
 250 cosmic ray model uncertainties. Atmospheric density un\_<sup>298</sup>  
 251 certainties are a subleading effect. We thus parametrize<sup>299</sup>  
 252 it as a linear function,  $\mathcal{F}(\delta)$ , which is obtained by fitting<sup>300</sup>  
 253 fluxes calculated with different atmospheric profiles gen\_<sup>301</sup>  
 254 erated within constraints imposed by temperature data<sup>302</sup>  
 255 from the AIRS satellite [42].<sup>303</sup>

256 The central flux prediction for the analysis is the<sup>304</sup>  
 257 HKKM model with H3a knee correction [43–45]. Additional<sup>305</sup>  
 258 flux variants are calculated using the analytic air<sup>306</sup>  
 259 shower evolution code of [46–48]. The cosmic spectrum<sup>308</sup>  
 260 variants considered are the Gaisser-Hillas [45], Zatsepin-<sup>309</sup>  
 261 Sokolskaya [49], and Poly-gonato models [50]. The<sup>310</sup>  
 262 hadronic models considered are QGSJET-II-4 [51] and<sup>311</sup>  
 263 SIBYILL2.3 [52]. For each combination of hadronic and<sup>312</sup>  
 264 primary model, fluxes calculated in various atmospheric<sup>313</sup>  
 265 density profiles are used to derive the  $\mathcal{F}(\delta)$  parameteri-<sup>314</sup>  
 266 zation.<sup>315</sup>

## 267 Neutrino propagation and interaction uncertainties<sup>320</sup>

268 Two sets of neutrino propagation uncertainties are<sup>322</sup>  
 269 treated in the search. Neutrino oscillation and absorption<sup>323</sup>  
 270 effects both depend on the Earth density profile along<sup>324</sup>  
 271 the neutrino trajectory, which is parameterized by the<sup>325</sup>  
 272 PREM model [53]. Uncertainties in the Earth compo-<sup>326</sup>  
 273 sition and density are accounted for by creating per-<sup>327</sup>  
 274 turbations of the PREM and re-propagating the neutrino<sup>328</sup>  
 275 flux. The PREM variants are constructed under the con-<sup>329</sup>  
 276 straints that the Earth mass and moment of inertia are<sup>330</sup>  
 277 preserved, that the density gradient is always negative in<sup>331</sup>  
 278 the core and mantle regions, and that the local perturba-<sup>332</sup>  
 279 tion is never more than 10%. The effects of Earth model<sup>333</sup>  
 280 uncertainty on the final propagated neutrino spectrum<sup>334</sup>  
 281 are incorporated by minimizing over 9 discrete perturbed<sup>335</sup>  
 282 models.<sup>336</sup>

283 A further propagation uncertainty is the neutrino<sup>338</sup>  
 284 charged-current cross-section which, at these energies, is<sup>339</sup>  
 285 dominated by deep inelastic scattering (DIS). The uncer-<sup>340</sup>  
 286 tainty in the cross-sections arises from parton distribu-<sup>341</sup>  
 287 tion function (PDF) uncertainties. A parametrization of<sup>342</sup>  
 288 the cross-section uncertainty uses calculations [54] (see<sup>343</sup>  
 289 also [55]) based on three different PDF sets: HERAPDF<sup>344</sup>  
 290 [56], CT10 [57] and NNPDF [58]. In each case, sim-<sup>345</sup>  
 291 ulated neutrino interactions are re-weighted using true<sup>346</sup>  
 292 neutrino energy and inelasticity given calculated doubly-<sup>347</sup>  
 293 differential cross sections, and the analysis fit is run using<sup>348</sup>  
 294 the weighted sample.<sup>349</sup>

## Detector and ice uncertainties

The absolute optical module photon collection efficiency,  $\epsilon$ , has been measured in the laboratory [30]. However, shadowing by the DOM cable and unknown local optical conditions after deployment introduce an uncertainty in the optical efficiency *in situ*, leading to uncertainty in the detected energy and angular event distribution. Here  $\epsilon$  is treated as a continuous nuisance parameter and re-weighting techniques are used to correct Monte Carlo distributions to arbitrary values. We follow the method developed in [16, 31], implementing a penalized spline [59] fitted to Monte Carlo datasets generated at various DOM efficiency values. Variability of the optical efficiency induces changes in the detector energy scale. In practice, the best fit value is tightly constrained by the position of the energy peak in the final sample.

The IceCube ice model applied in this analysis has nearly a thousand free parameters that are minimized in an iterative fit procedure using LED flasher data [60]. The model implements vertically varying absorption and scattering coefficients across tilted isochronal ice layers. The fit procedure yields a systematic and statistical uncertainty on the optical scattering and absorption coefficients in the ice, as well as a larger uncertainty on the amount of light deposited by the LED flashers. This larger uncertainty was later reduced by introducing azimuthal anisotropy in the scattering length into the ice model, which may result from dust grain shear due to glacial flow [61]. We use the model described in [60] as the central ice model, and then use the model with anisotropy [61] as an alternative to assess the impact of this effect. We also incorporate models with 10% variations in the optical absorption and scattering coefficients to account for the uncertainty on those parameters. A full Monte Carlo sample is created for each model variation.

The ice column immediately surrounding the DOMs has different optical properties than the bulk ice due to dissolved gases that are trapped during the refreezing process following DOM deployment. This introduces additional scattering near the DOM and has a nontrivial effect on its angular response [60]. To quantify this effect on the final event distribution, a comparison is made between the extreme case of the DOM assumed to have its laboratory-derived angular response vs. the nominal hole ice model as discrete ice model variants.

## RESULTS

The analysis detailed here was developed with 90% of the data sample held blind, and unblinding was a multi-step process. The agreement of Monte Carlo (MC) simulations based on the no-steriles hypothesis (corresponding to more than 360 years of simulated data) with

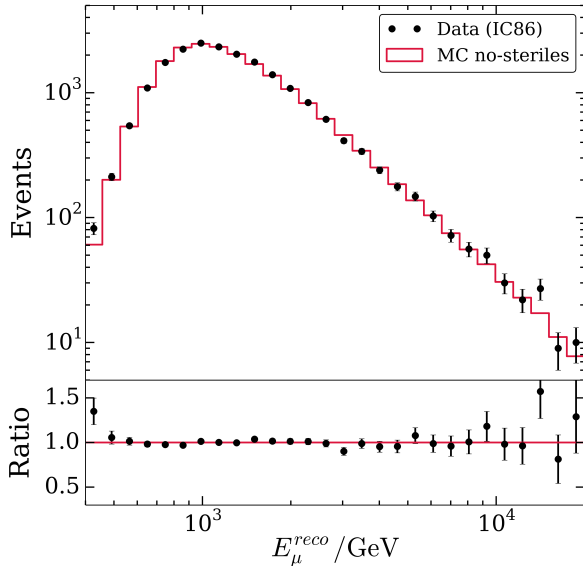


FIG. 2. Reconstructed energy distribution in data and Monte Carlo for the no-steriles hypothesis in the analysis.

347 data was evaluated using one-dimensional energy and  
 348 zenith angle distributions, which would wash out the  
 349 resonance signature of sterile neutrinos (Fig. 2). Good  
 350 data-MC consistency was observed and no nuisance pa-  
 351 rameter was found to have a significant pull outside of its  
 352 prior. Other comparisons, insensitive to the sterile neu-  
 353 trino signature, were made by examining subsets of the  
 354 data split by reconstructed azimuthal track angle, and by  
 355 event center-of-gravity. No significant data-Monte Carlo  
 356 disagreements were observed. The full event distribution  
 357 in the two-dimensional analysis space, and the pulls-per-  
 358 bin from the null hypothesis (Fig. 3) were then examined.  
 359 Event-by-event reconstructed data and Monte Carlo can  
 360 be found in [62].

361 The LLH value for the data given each sterile neutrino  
 362 hypothesis was calculated. No evidence for sterile neutrino-  
 363 nos was observed. The best fit of the blind, shape-only  
 364 analysis is at  $\Delta m^2 = 10 \text{ eV}^2$  and  $\sin^2 2\theta_{24} = 0.56$  with a  
 365 log likelihood difference from the no-steriles hypothesis of  
 366  $\Delta \text{LLH} = 1.91$ , corresponding to a p-value of 15%. Since  
 367 the fit does not constrain flux normalization, LLH min-  
 368 ima at  $\Delta m^2 \gtrsim 5 \text{ eV}^2$  are highly degenerate with the no-  
 369 sterile hypothesis. This is because the oscillation effect  
 370 becomes a fast vacuum-like oscillation smeared out by  
 371 the energy resolution of the detector, and thus changes  
 372 the normalization but has no effect on shape.

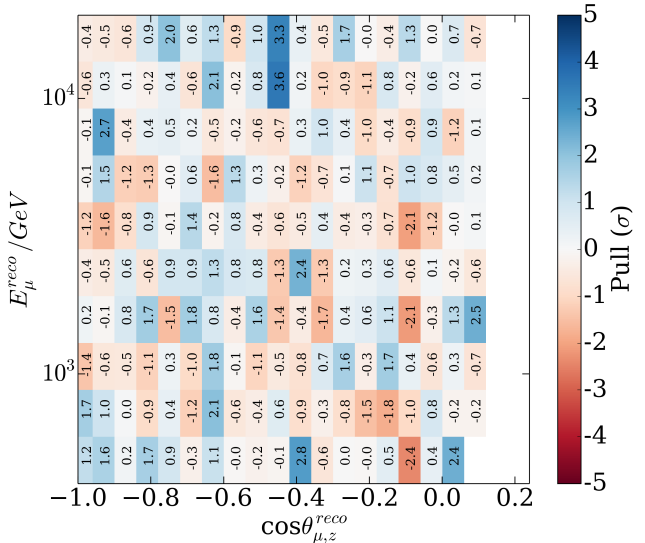


FIG. 3. The statistical-only pulls (shape+rate analysis) per reconstructed energy and zenith angle bin at the best nuisance parameter fit point for the no-sterile hypothesis. Shown empty bins are those that were evaluated in the analysis but had no data events remaining following cuts.

cases, slightly stronger exclusion limits can be found by increasing the search space to higher mass. Second, the degeneracy between normalization and mixing can lead to unphysical values for the normalization that compensate for the sterile neutrino oscillation effect. To avoid these ambiguities, an extension of the analysis (denoted rate+shape) was developed to constrain the neutrino flux normalization using a prior with 40% uncertainty in the likelihood function, based on [44, 63]. This results in a weakened exclusion relative to the blind analysis proposal. However, since it is more robust, we consider it our primary result. For the rate+shape analysis, the best fit is at  $\Delta m^2 = 10 \text{ eV}^2$  and  $\sin^2 2\theta_{24} = 0.50$ , with a log likelihood difference from the no-steriles hypothesis of  $\Delta \text{LLH} = 0.75$ , corresponding to a p-value of 47%. This minimum is unique under extension of the analysis space to higher masses, since the large  $\Delta m^2$  region is no longer degenerate with the no-sterile hypothesis. This was checked over an extended parameter space up to  $\Delta m^2 = 100 \text{ eV}^2$ . The confidence interval for the shape-only and the rate+shape analyses are shown in Fig. 4.

A number of checks of the rate+shape analysis result were made (see [40]). The exclusion is found to be robust under tightening or loosening the nuisance parameter priors by a factor of two. Different strengths of the normalization constraint were tested, and the result was found to be relatively insensitive to values between 30% and 50%. The pulls on each continuous nuisance parameter were evaluated at all points in the LLH space and found to behave as expected. The contour was redrawn for each discrete nuisance variant and found to have good

stability. The Wilks confidence intervals [64] were validated using Feldman-Cousins ensembles along the contour [39] and found to be accurate frequentist confidence intervals.

An independent search was conducted using the 59-string IceCube data [65, 66], introduced previously, that also finds no evidence of sterile neutrinos. The IC59 analysis, described in detail in [17], used different treatments for the systematic uncertainties, for the fitting methods and employed independent Monte Carlo samples that were compared to data using unique weighting methods. In particular, the event selection used for this data set had higher efficiency for low-energy neutrinos, using a threshold at 320 GeV, extending the sensitivity of the analysis to smaller  $\Delta m^2$ . However, detailed *a posteriori* inspections revealed that a background contamination from cosmic ray induced muons, on the level of 0.3% of the full sample, is largest in this region and could lead to an artificially strong exclusion limit. Further, the energy reconstruction algorithm used in both analyses, which measures the level of bremsstrahlung and other stochastic light emission along the muon track, is vulnerable to subtle detector modeling issues and suffers degraded energy resolution in the low-energy region where most muons are minimum-ionizing tracks and a large fraction either start or stop within the detector. It was therefore decided to exclude these events to avoid biasing the resulting exclusion regions. As a result of this *a posteriori* change, the IC59 analysis retains a comparable range of sensitivity in  $\Delta m^2$  but the reach in  $\sin^2 \theta_{24}$  is strongly reduced (see Fig. 4). However, we still present this result as it independently confirms the result presented here.

## DISCUSSION AND CONCLUSION

Resonant oscillations due to matter effects would produce distinctive signatures of sterile neutrinos in the large set of high energy atmospheric neutrino data recorded by the IceCube Neutrino Observatory. The IceCube collaboration has performed searches for sterile neutrinos with  $\Delta m^2$  between 0.1 and 10 eV<sup>2</sup>. We have assumed a minimal set of flavor mixing parameters in which only  $\theta_{24}$  is non-zero.

A nonzero value for  $\theta_{34}$  would change the shape of the MSW resonance while increasing the total size of the disappearance signal [25]. As discussed in [27], among the allowed values of  $\theta_{34}$  [8], the model with  $\theta_{34}=0$  presented here leads to the most conservative exclusion in  $\theta_{24}$ . The angle  $\theta_{14}$  is tightly constrained by electron neutrino disappearance measurements [12], and nonzero values of  $\theta_{14}$  within the allowed range do not strongly affect our result.

Figure 5 shows the current IceCube results at 90% and 99% confidence levels, with predicted sensitivities, compared with 90% confidence level exclusions from previous disappearance searches [7–10]. Our exclusion con-

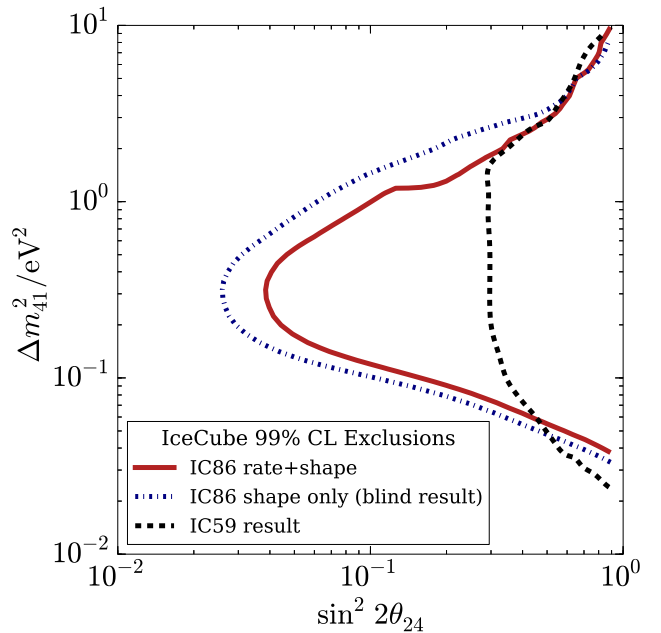


FIG. 4. Results from IceCube sterile neutrino searches (regions to the right of the contours are excluded). The dot-dashed blue line shows the result of the original analysis based on shape alone, while the solid red line shows the final result with a normalization prior included to prevent degeneracies between the no-steriles hypothesis and sterile neutrinos with masses outside the range of sensitivity. The dashed black line is the exclusion range derived from an independent analysis of data from the 59-string IceCube configuration.

tour is essentially contained within the expected +/- 95% range around the projected sensitivity derived from simulated experiments, assuming a no-steriles hypothesis. In any single realization of the experiment, deviations from the mean sensitivity are expected due to statistical fluctuations in the data and, to a considerably lesser extent, in the Monte Carlo data sets. Also shown is the 99% allowed region from a fit to the short baseline appearance experiments, including LSND and MiniBooNE, from [12, 13, 25], projected with  $|U_{e4}|^2$  fixed to its world best fit value according to two global fit analyses [12, 13]. This region is excluded at approximately the 99% confidence level, further increasing tension with the short baseline anomalies, and removing much of the remaining parameter space of the 3+1 model. We note that the methods developed for the IC59 and IC86 analyses are being applied to additional data sets, including several years of data already recorded by IceCube, from which we anticipate improvements in IceCubes sterile neutrino sensitivity.

We acknowledge the support from the following agencies: U.S. National Science Foundation-Office of Polar Programs, U.S. National Science Foundation-Physics Division, University of Wisconsin Alumni Research Foundation, the Grid Laboratory Of Wisconsin

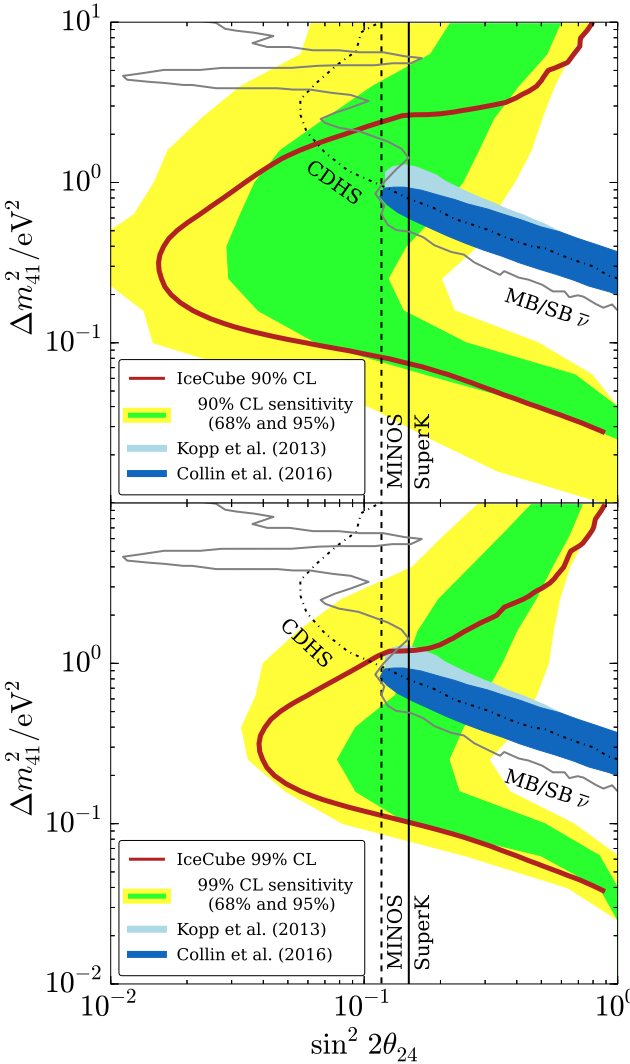


FIG. 5. Results from the IceCube search. (Top) The 90% (orange solid line) CL contour is shown with bands containing 68% (green) and 95% (yellow) of the 90% contours in simulated pseudo-experiments, respectively. (Bottom) The 99% (red solid line) CL contour is shown with bands containing 68% (green) and 95% (yellow) of the 99% contours in simulated pseudo-experiments, respectively. The contours and bands are overlaid on 90% CL exclusions from previous experiments [7–10], and the 99% CL allowed region from global fits to appearance experiments including MiniBooNE and LSND, assuming  $|U_{e4}|^2 = 0.023$  [12] and  $|U_{e4}|^2 = 0.027$  [13] respectively.

ture for Computing (SNIC), and Knut and Alice Wallenberg Foundation, Sweden; German Ministry for Education and Research (BMBF), Deutsche Forschungsgemeinschaft (DFG), Helmholtz Alliance for Astroparticle Physics (HAP), Research Department of Plasmas with Complex Interactions (Bochum), Germany; Fund for Scientific Research (FNRS-FWO), FWO Odysseus programme, Flanders Institute to encourage scientific and technological research in industry (IWT), Belgian Federal Science Policy Office (Belspo); University of Oxford, United Kingdom; Marsden Fund, New Zealand; Australian Research Council; Japan Society for Promotion of Science (JSPS); the Swiss National Science Foundation (SNSF), Switzerland; National Research Foundation of Korea (NRF); Villum Fonden, Danish National Research Foundation (DNRF), Denmark

Note added: During the publication process of this paper, an analysis using IceCube public data [67] was performed (see following letter). Though this independent analysis has a limited treatment of systematics, it follows the technique described here and in refs. [40, 41], and obtains comparable bounds. To allow for better reproduction of the result shown in this paper in the future, we have put forward a data release that incorporates detector systematics [62].

\* Earthquake Research Institute, University of Tokyo, Bunkyo, Tokyo 113-0032, Japan

† Instituto de Física Corpuscular, Universidad de Valencia CSIC, Valencia 46071, Spain

‡ NASA Goddard Space Flight Center, Greenbelt, MD 20771, USA

<sup>§</sup> please direct correspondence to: analysis@icecube.wisc.edu

- [1] C. Athanassopoulos *et al.* (LSND), *Phys. Rev. Lett.* **77**, 3082 (1996), arXiv:nucl-ex/9605003 [nucl-ex].
- [2] A. Aguilar-Arevalo *et al.* (LSND), *Phys. Rev.* **D64**, 112007 (2001), arXiv:hep-ex/0104049 [hep-ex].
- [3] A. A. Aguilar-Arevalo *et al.* (MiniBooNE), *Phys. Rev. Lett.* **110**, 161801 (2013), arXiv:1207.4809 [hep-ex].
- [4] G. Mention, M. Fechner, T. Lasserre, T. A. Mueller, D. Lhuillier, M. Cribier, and A. Letourneau, *Phys. Rev.* **D83**, 073006 (2011), arXiv:1101.2755 [hep-ex].
- [5] J. N. Bahcall, P. I. Krastev, and E. Lisi, *Phys. Lett.* **B348**, 121 (1995), arXiv:hep-ph/9411414 [hep-ph].
- [6] B. Armbruster *et al.* (KARMEN), *Phys. Rev.* **D65**, 112001 (2002), arXiv:hep-ex/0203021 [hep-ex].
- [7] K. Abe *et al.* (Super-Kamiokande), *Phys. Rev.* **D91**, 052019 (2015), arXiv:1410.2008 [hep-ex].
- [8] P. Adamson *et al.* (MINOS), *Phys. Rev. Lett.* **107**, 011802 (2011), arXiv:1104.3922 [hep-ex].
- [9] G. Cheng *et al.* (SciBooNE, MiniBooNE), *Phys. Rev.* **D86**, 052009 (2012), arXiv:1208.0322.
- [10] F. Dydak *et al.*, *Phys. Lett.* **B134**, 281 (1984).
- [11] C. Giunti and M. Laveder, *Phys. Rev.* **D84**, 073008 (2011), arXiv:1107.1452 [hep-ph].
- [12] J. Kopp, P. A. N. Machado, M. Maltoni, and T. Schwetz,

- 555 JHEP **05**, 050 (2013), arXiv:1303.3011 [hep-ph]. 619
- 556 [13] J. M. Conrad, C. M. Ignarra, G. Karagiorgi, M. H. Shae-620  
557 vitz, and J. Spitz, *Adv. High Energy Phys.* **2013**, 163897621  
558 (2013), arXiv:1207.4765 [hep-ex]. 622
- 559 [14] F. Halzen and S. R. Klein, *Rev. Sci. Instrum.* **81**, 081101623  
560 (2010), arXiv:1007.1247 [astro-ph.HE]. 624
- 561 [15] M. C. Gonzalez-Garcia, F. Halzen, and M. Maltoni,625  
562 *Phys. Rev. D* **71**, 093010 (2005), arXiv:hep-ph/0502223626  
563 [hep-ph]. 627
- 564 [16] M. G. Aartsen *et al.* (IceCube), *Phys. Rev. Lett.* **115**,628  
565 081102 (2015), arXiv:1507.04005 [astro-ph.HE]. 629
- 566 [17] M. G. Aartsen *et al.* (IceCube), *Phys. Rev. D* **89**, 062007630  
567 (2014), arXiv:1311.7048 [astro-ph.HE]. 631
- 568 [18] H. Nunokawa, O. L. G. Peres, and R. Zukanovich Fun-632  
569 chal, *Phys. Lett. B* **562**, 279 (2003), arXiv:hep-633  
570 ph/0302039 [hep-ph]. 634
- 571 [19] K. N. Abazajian *et al.*, (2012), arXiv:1204.5379 [hep-ph].635
- 572 [20] S. Choubey, *JHEP* **12**, 014 (2007), arXiv:0709.1937 [hep-636  
573 ph]. 637
- 574 [21] S. Razzaque and A. Yu. Smirnov, *JHEP* **07**, 084 (2011),638  
575 arXiv:1104.1390 [hep-ph]. 639
- 576 [22] V. Barger, Y. Gao, and D. Marfatia, *Phys. Rev. D* **85**,640  
577 011302 (2012), arXiv:1109.5748 [hep-ph]. 641
- 578 [23] A. Esmaili, F. Halzen, and O. L. G. Peres, *JCAP* **1211**,642  
579 041 (2012), arXiv:1206.6903 [hep-ph]. 643
- 580 [24] S. Razzaque and A. Yu. Smirnov, *Phys. Rev. D* **85**,644  
581 093010 (2012), arXiv:1203.5406 [hep-ph]. 645
- 582 [25] A. Esmaili and A. Yu. Smirnov, *JHEP* **12**, 014 (2013),646  
583 arXiv:1307.6824 [hep-ph]. 647
- 584 [26] A. Esmaili, F. Halzen, and O. L. G. Peres, *JCAP* **1307**,648  
585 048 (2013), arXiv:1303.3294 [hep-ph]. 649
- 586 [27] M. Lindner, W. Rodejohann, and X.-J. Xu, *JHEP* **01**,650  
587 124 (2016), arXiv:1510.00666 [hep-ph]. 651
- 588 [28] K. Hanson and O. Tarasova (IceCube), *BEAUNE 2005*652  
589 *New Developments in Photodetection*, *Nucl. Instrum. Meth.* **A567**, 214 (2006). 653
- 590 [29] R. Abbasi *et al.* (IceCube), *Nucl. Instrum. Meth.* **A601**,655  
591 294 (2009), arXiv:0810.4930 [physics.ins-det]. 656
- 592 [30] R. Abbasi *et al.* (IceCube), *Nucl. Instrum. Meth.* **A618**,657  
593 139 (2010), arXiv:1002.2442 [astro-ph.IM]. 658
- 594 [31] C. Weaver, *Evidence for Astrophysical Muon Neutrinos*659  
595 *from the Northern Sky*, Ph.D. thesis, University of Wis-660  
596 consin, Madison (2015). 661
- 597 [32] M. G. Aartsen *et al.* (IceCube), *Phys. Rev. D* **91**, 022001662  
598 (2015), arXiv:1410.1749 [astro-ph.HE]. 663
- 599 [33] J. Ahrens *et al.* (AMANDA), *Nucl. Instrum. Meth.* **523**664  
600 (2004). 665
- 601 [34] M. G. Aartsen *et al.* (IceCube), *JINST* **9**, P03009 (2014),666  
602 arXiv:1311.4767 [physics.ins-det]. 667
- 603 [35] C. A. Argüelles Delgado, J. Salvado, and C. N. Weaver,668  
604 (2014), arXiv:1412.3832 [hep-ph]. 669
- 605 [36] C. A. Argüelles Delgado, J. Salvado, and C. N.670  
606 Weaver, “SQuIDS,” <https://github.com/jsalvado/SQuIDS> (2015). 671
- 607 [37] C. A. Argüelles Delgado, J. Salvado, and C. N.673  
608 Weaver, “ $\nu$ -SQuIDS,” <https://github.com/Arguelles/nuSQuIDS> (2015). 674
- 609 [38] M. Wallraff and C. Wiebusch, *Comput. Phys. Commun.* **197**, 185 (2015), arXiv:1409.1387 [astro-ph.IM]. 675
- 610 [39] G. J. Feldman and R. D. Cousins, *Phys. Rev. D* **57**, 3873678  
611 (1998), arXiv:physics/9711021 [physics.data-an]. 679
- 612 [40] B. J. P. Jones, *Sterile Neutrinos in Cold Climates*, Ph.D.680  
613 thesis, MIT (2015). 681
- 614 [41] C. A. Argüelles Delgado, *New Physics with Atmospheric*682  
615 *Neutrinos*, Ph.D. thesis, University of Wisconsin at Madison (2015).
- 616 [42] B. Tian and National Center for Atmospheric Research Staff (Eds), “The Climate Data Guide: AIRS and AMSU: Tropospheric air temperature and specific humidity,” (2015).
- 617 [43] T. Sanuki, M. Honda, T. Kajita, K. Kasahara, and S. Midorikawa, *Phys. Rev. D* **75**, 043005 (2007), arXiv:astro-ph/0611201 [astro-ph].
- 618 [44] M. Honda, T. Kajita, K. Kasahara, S. Midorikawa, and T. Sanuki, *Phys. Rev. D* **75**, 043006 (2007), arXiv:astro-ph/0611418 [astro-ph].
- 619 [45] T. K. Gaisser, T. Stanev, and S. Tilav, *Front.Phys.China* **8**, 748 (2013), arXiv:1303.3565 [astro-ph.HE].
- 620 [46] A. Fedynitch, R. Engel, T. K. Gaisser, F. Riehn, and T. Stanev, *18th International Symposium on Very High Energy Cosmic Ray Interactions (ISVHE-CRI 2014) Geneva, Switzerland, August 18-22, 2014*, (2015), 10.1051/epjconf/20159908001, [EPJ Web Conf.99,08001(2015)], arXiv:1503.00544 [hep-ph].
- 621 [47] A. Fedynitch, “MCEq,” <https://github.com/afedynitch/MCEq>.
- 622 [48] G. H. Collin and J. M. Conrad, “An estimation of systematics for up-going atmospheric neutrino flux at the south pole,” <http://dspace.mit.edu/handle/1721.1/98078> (2015).
- 623 [49] V. I. Zatsepin and N. V. Sokolskaya, *Astron. Astrophys.* **458**, 1 (2006), arXiv:astro-ph/0601475 [astro-ph].
- 624 [50] J. R. Hoerandel, *Astropart. Phys.* **19**, 193 (2003), arXiv:astro-ph/0210453 [astro-ph].
- 625 [51] S. Ostapchenko, *Phys. Rev. D* **83**, 014018 (2011), arXiv:1010.1869 [hep-ph].
- 626 [52] F. Riehn, R. Engel, A. Fedynitch, T. K. Gaisser, and T. Stanev, (2015), arXiv:1510.00568 [hep-ph].
- 627 [53] A. M. Dziewonski and D. L. Anderson, *Physics of the Earth and Planetary Interiors* **25**, 297 (1981).
- 628 [54] A. Cooper-Sarkar, P. Mertsch, and S. Sarkar, *JHEP* **08**, 042 (2011), arXiv:1106.3723 [hep-ph].
- 629 [55] C. A. Argüelles Delgado, M. Kroll, F. Halzen, and J. Tjus, “New NNLO calculation of the high energy neutrino cross section with LHC pdfs,” In preparation.
- 630 [56] F. D. Aaron *et al.* (ZEUS, H1), *JHEP* **01**, 109 (2010), arXiv:0911.0884 [hep-ex].
- 631 [57] J. Gao, M. Guzzi, J. Huston, H.-L. Lai, Z. Li, P. Nadolsky, J. Pumplin, D. Stump, and C. P. Yuan, *Phys. Rev. D* **89**, 033009 (2014), arXiv:1302.6246 [hep-ph].
- 632 [58] E. R. Nocera, R. D. Ball, S. Forte, G. Ridolfi, and J. Rojo (NNPDF), *Nucl. Phys. B* **887**, 276 (2014), arXiv:1406.5539 [hep-ph].
- 633 [59] N. Whitehorn, J. van Santen, and S. Lafebre, *Comput. Phys. Commun.* **184**, 2214 (2013), arXiv:1301.2184 [physics.data-an].
- 634 [60] M. G. Aartsen *et al.* (IceCube), *Nucl. Instrum. Meth. A* **711**, 73 (2013), arXiv:1301.5361 [astro-ph.IM].
- 635 [61] M. G. Aartsen *et al.* (IceCube), (2013), arXiv:1309.7010 [astro-ph.HE].
- 636 [62] <http://icecube.wisc.edu/science/data/access>.
- 637 [63] A. Fedynitch, J. Becker Tjus, and P. Desiati, *Phys. Rev. D* **86**, 114024 (2012), arXiv:1206.6710 [astro-ph.HE].
- 638 [64] K. A. Olive *et al.* (Particle Data Group), *Chin. Phys. C* **38**, 090001 (2014).
- 639 [65] M. G. Aartsen *et al.* (IceCube) (2015) arXiv:1510.05227 [astro-ph.HE].
- 640 [66] M. Wallraff, Ph.D. thesis, RWTH Aachen (in prepara-

683 tion).

684 [67] [http://icecube.wisc.edu/science/data/HE\\_NuMu\\_](http://icecube.wisc.edu/science/data/HE_NuMu_)  
685 **diffuse.**